

Coordination Tuning of Metal Porphyrins for Improved Oxygen Evolution Reaction

Haoyuan Lv⁺, Xue-Peng Zhang⁺, Kai Guo, Jinxiu Han, Hongbo Guo, Haitao Lei, Xialiang Li, Wei Zhang, Ulf-Peter Apfel, and Rui Cao*

Abstract: The nucleophilic attack of water or hydroxide on metal-oxo units forms an O–O bond in the oxygen evolution reaction (OER). Coordination tuning to improve this attack is intriguing but has been rarely realized. We herein report on improved OER catalysis by metal porphyrin **1-M** ($M=Co, Fe$) with a coordinatively unsaturated metal ion. We designed and synthesized **1-M** by sterically blocking one porphyrin side with a tethered tetraazacyclododecane unit. With this protection, the metal-oxo species generated in OER can maintain an unoccupied *trans* axial site. Importantly, **1-M** displays a higher OER activity in alkaline solutions than analogues lacking such an axial protection by decreasing up to 150-mV overpotential to achieve 10 mA/cm^2 current density. Theoretical studies suggest that with an unoccupied *trans* axial site, the metal-oxo unit becomes more positively charged and thus is more favoured for the hydroxide nucleophilic attack as compared to metal-oxo units bearing *trans* axial ligands.

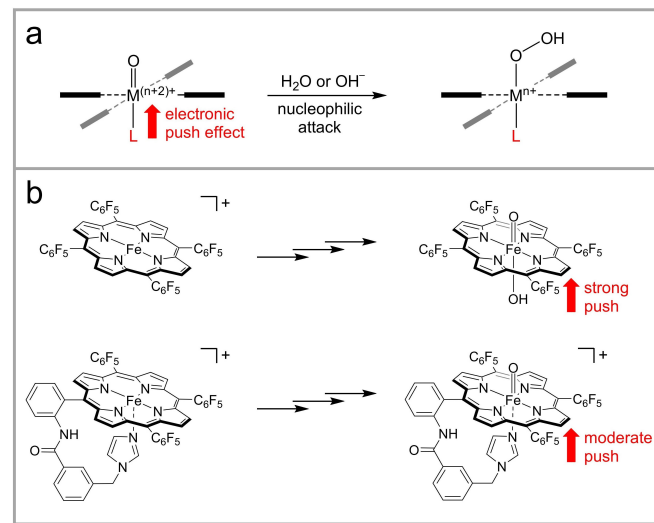


Figure 1. (a) The electronic "push effect" of *trans* axial ligands on the O–O bond formation via nucleophilic attacks. (b) Axial coordination tuning to control the oxo electron density.

The oxygen evolution reaction (OER) is a fundamental process in natural and artificial energy conversion schemes.^[1–5] Due to the slow kinetics of OER, efficient catalysts are required.^[6–17] Terminal metal-oxo species are generally considered as intermediates in OER.^[18–20] The nucleophilic attack of water or hydroxide on metal-oxo is a possible O–O bond formation process (Figure 1a).^[21–27] As the coordination environment of a metal ion controls the metal-oxo reactivity, tuning the coordination to make metal-oxo more active towards nucleophilic attack is an intriguing way to improve OER. However, although many transition

metal complexes, including those of Mn,^[26,28–30] Fe,^[27,31–34] Co,^[35–40] Ni,^[41–43] and Cu,^[44–47] have been identified as molecular OER catalysts, few studies have been shown to improve O–O bond formation via rational coordination tuning of metal ions.^[27]

Axial ligands can significantly affect the reactivity of its *trans* metal-oxo units via an electronic "push effect" (Figure 1a).^[48–51] With strong electron-donating axial ligands, the electron density of the oxo increases, which is unfavoured for nucleophilic attack. To decrease the electron density of metal-oxo units, we recently reported a Fe porphyrin tethered with an imidazole group for Fe axial binding.^[27] Because of the planar structure, the metal ion in porphyrins has two axial sites *trans* to each other. During OER under alkaline conditions, one axial site eventually becomes an Fe-oxo unit, while its *trans* axial site coordinates a hydroxide. By using an imidazole ligand to protect the *trans* axial site of the Fe-oxo unit (Figure 1b), Fe porphyrin became more active for OER. Compared to negatively charged hydroxide, imidazole is neutral in charge and has a smaller electron-pushing effect, making formal $Fe^{\text{V}}=\text{O}$ relatively more electron-deficient for nucleophilic attack.

In order to further improve OER catalysis, we herein report on the synthesis of metal porphyrin **1-M** ($M=Co, Fe$) with a sterically blocked axial site (Figure 2a). By using a

[*] H. Lv,⁺ Dr. X.-P. Zhang,⁺ K. Guo, J. Han, H. Guo, Dr. H. Lei, Dr. X. Li, Prof. Dr. W. Zhang, Prof. Dr. R. Cao
Key Laboratory of Applied Surface and Colloid Chemistry, Ministry of Education, School of Chemistry and Chemical Engineering, Shaanxi Normal University
710119 Xi'an (China)
E-mail: ruicao@snnu.edu.cn

Prof. Dr. U.-P. Apfel
Ruhr-Universität Bochum, Fakultät für Chemie und Biochemie, Anorganische Chemie I
Universitätsstrasse 150, 44801 Bochum (Germany)
and
Fraunhofer UMSICHT
Osterfelder Strasse 3, 46047 Oberhausen (Germany)

[+] These authors contributed equally to this work.

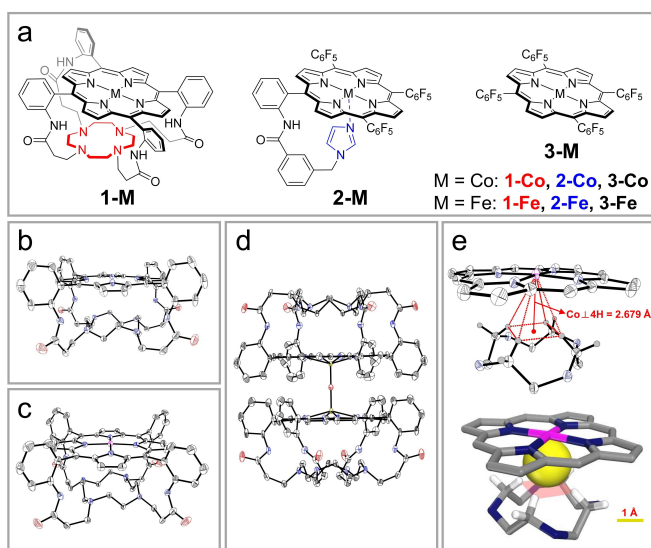


Figure 2. (a) Molecular structures of **1-M**, **2-M** and **3-M** ($M = \text{Co, Fe}$). Thermal ellipsoid plots (30% probability) of the X-ray structure of the cyclen-modified metal-free porphyrin (b), **1-Co** (c), and **1-Fe** dimer (d). The axial methanol molecule in **1-Co** and the hydrogen atoms in all three structures are omitted for clarity. (e) The size of the cavity flanked by the two macrocycles.

tetraazacyclododecane (also known as cyclen) moiety to protect one porphyrin side, the protected metal axial site will keep unoccupied in OER. We also synthesized **2-M** ($M = \text{Co, Fe}$) and **3-M** ($M = \text{Co, Fe}$) (Figure 2a). Electrocatalytic studies gave an OER activity order of **1-M** > **2-M** > **3-M**. Importantly, theoretical studies suggested that metal-oxo with an unoccupied *trans* axial site is more positively charged and is more favoured for hydroxide nucleophilic attack as compared to metal-oxo units bearing *trans* axial ligands. This work is significant to show enhanced O–O bond formation through axial coordination tuning and to present an unparalleled strategy to make coordinatively unsaturated metal porphyrins for improved OER.

Metal porphyrins **1-M** were synthesized (Scheme S1). First, the cyclen-modified metal-free porphyrin was synthesized. Its high-resolution mass spectrometry (HRMS) showed an ion at a mass-to-charge ratio of 1063.5082 (Figure S3). The structure of this metal-free porphyrin was studied (Figure 2b),^[52] confirming that one porphyrin side is sterically protected by a cyclen unit. Due to the strain of the cyclen, the lone pairs of its four N atoms directs away from each other and are not able to chelate metal ions. The reaction of this metal-free porphyrin with Co^{II} and Fe^{II} salts gave **1-Co** and **1-Fe**, respectively. The HRMS of **1-Co** (1120.4264, Figure S4) and the triflate salt of **1-Fe** (1116.4198, Figure S5) confirmed their identity and purity.

High-quality crystals of **1-Co** for X-ray diffraction studies were obtained (Figure 2c).^[53] The Co ion is coordinated at the center of the porphyrin via four Co–N bonds (1.978 (3) Å, by average). One methanol molecule binds at the unprotected axial site of Co with a Co–O distance of 2.008(10) Å. Bond valence sum and charge balance calculations suggested a Co^{II} ion. The cyclen does not bind any

metal ion although a large excess of Co^{II} is used in the synthesis. The cavity flanked by the porphyrin and cyclen is very small (Figure 2e). The distance between Co ion and the equatorial plane defined by the four H atoms of the cyclen methylene groups is 2.679 Å. This short distance and the small cavity indicate that it is not likely to have an axial ligand at the protected side of Co.

We tried to grow crystals of **1-Fe**. However, our attempts gave a dimerized structure, which has two **1-Fe** units bridged through a Fe–O–Fe bond (Figure 2d).^[54] The dimer is located at the special position with a C_4 axis passing through the Fe–O–Fe atoms. Thus, the Fe–O–Fe bond angle is 180° with two Fe–O bonds of 1.750(14) Å and 1.763(14) Å. For each **1-Fe** unit, the Fe ion is chelated by the porphyrin via four N atoms. The Fe–N bond length is 2.075(6) Å for Fe1 and 2.086(6) Å for Fe2, suggesting two Fe^{III} atoms. Similarly, the cyclen does not bind any metal ion, and the axial site of Fe at the protected side is unoccupied. Note that discrete **1-Fe** instead of dimer was obtained in synthesis as confirmed by HRMS (Figure S5) and UV/Vis (Figure 3). The dimerization of Fe porphyrins usually occurred during crystal growths.^[55] As controls, **2-M** and **3-M** ($M = \text{Co, Fe}$) were synthesized according to the methods we recently reported (Figure S6–S9).^[27,56]

Structural analysis of **1-M** suggested that the cyclen-protected side of metal ions cannot bind axial ligands. Moreover, we studied the coordination of **1-Fe**. We designed

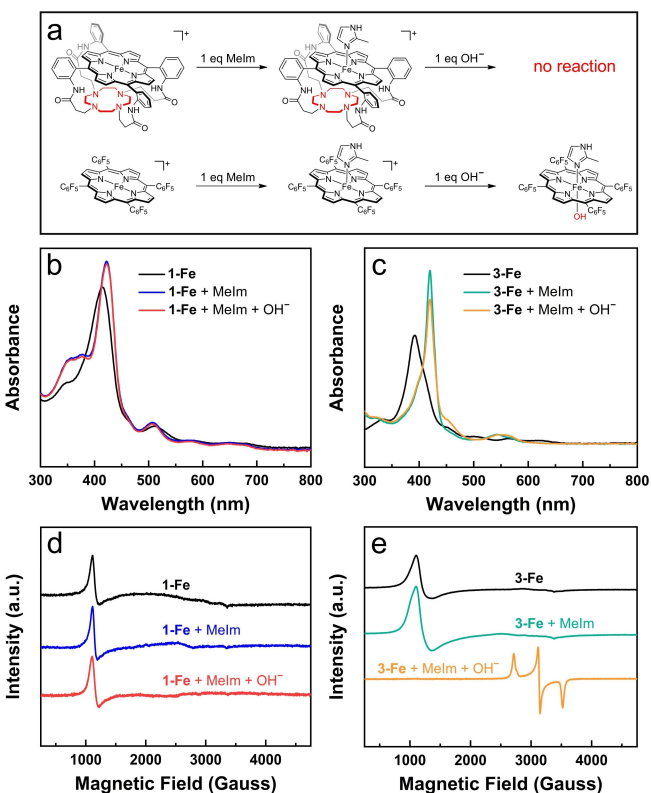


Figure 3. (a) The reaction of **1-Fe** and **3-Fe** by adding Melm and hydroxide. The UV/Vis spectra of **1-Fe** (b) and **3-Fe** (c) and the EPR spectra of **1-Fe** (d) and **3-Fe** (e) in tetrahydrofuran with the addition of Melm and hydroxide. EPR spectra were measured at 100 K.

a reaction sequence of **1-Fe** with methylimidazole (MeIm) and then with hydroxide (Figure 3a). By adding one equivalent of MeIm, the UV/Vis spectrum of **1-Fe** showed notable changes, indicating MeIm coordination on Fe (Figure 3b). Because of its large size, MeIm will bind at the unprotected axial site of Fe. Similar UV/Vis changes were observed by adding one equivalent of MeIm to **3-Fe** (Figure 3c). Next, hydroxide was added to the MeIm-treated **1-Fe**, showing no changes in UV/Vis (Figure 3b). However, the addition of hydroxide to MeIm-treated **3-Fe** led to further changes (Figure 3c). These results are consistent with the structural differences of **1-Fe** and **3-Fe**. We also studied these reactions by electron paramagnetic resonance (EPR). After adding MeIm and hydroxide, the EPR spectrum of **1-Fe** gave only high-spin Fe^{III} signals (Figure 3d), while the EPR spectrum of **3-Fe** gave low-spin Fe^{III} signals (Figure 3e).^[27,57,58] We considered that with MeIm and hydroxide, a five-coordinate high-spin Fe^{III} was obtained for **1-Fe**, while a six-coordinate low-spin Fe^{III} could be obtained for **3-Fe**. Therefore, we confirmed that the cyclen-protected side of **1-Fe** has sufficient steric hindrance to exclude hydroxide ions, making this protected axial site of **1-Fe** unoccupied under alkaline conditions.

The redox properties of **1-Co** and **1-Fe** were then studied. The cyclic voltammogram (CV) of **1-Co** in dimethylformamide showed two reduction waves (Figure S15), which are comparable to those of **2-Co** and **3-Co** (Table S1). For **1-Fe**, its CV displayed three reduction waves (Figure S19), which were also comparable to those of **2-Fe** and **3-Fe** (Table S2). These results suggest that **1-M** has similar redox properties as **2-M** and **3-M**. The reduction peak currents of **1-Co** and **1-Fe** showed linear dependence on the square root of scan rates, giving a diffusion coefficient of $D_{1-Co} = 3.77 \times 10^{-6} \text{ cm}^2/\text{s}$ (Figure S23, S24) and $D_{1-Fe} = 3.57 \times 10^{-6} \text{ cm}^2/\text{s}$ (Figure S25, S26). The similarity of the diffusion coefficient of **1-Co** and **1-Fe** further suggests that the monomer instead of the dimer of **1-Fe** presents in the solution.

Electrocatalytic OER were studied in 1.0 M KOH solutions. Metal porphyrins were first loaded on carbon nanotubes (CNTs), which was confirmed by using X-ray photoelectron spectroscopy and energy dispersive X-ray spectroscopy (Figure S27–S30). Scanning electron microscopy and transmission electron microscopy analyses showed no aggregated particles in the resulted hybrid materials (Figure S32). As shown in Figure 4a, the linear sweep voltammogram (LSV) of **1-Co** displayed a high activity for electrocatalytic OER by reaching a 10 mA/cm² current density at an overpotential of $\eta_{10} = 390 \text{ mV}$ (Figure 4c). This activity is higher than that of **2-Co** ($\eta_{10} = 450 \text{ mV}$) and **3-Co** ($\eta_{10} = 540 \text{ mV}$). Note that unmodified carbon nanotubes exhibited very poor OER activity (Figure S33, S34). All potentials reported in aqueous solutions are referenced to the reversible hydrogen electrode (RHE). Similarly, **1-Fe** outperforms **2-Fe** and **3-Fe** for OER (Figure 4b). The η_{10} values are 430 mV for **1-Fe**, 460 mV for **2-Fe**, and 530 mV for **3-Fe** (Figure 4d).

The OER Tafel slope was measured, indicating that **1-Co** and **1-Fe** have better OER kinetics as compared to

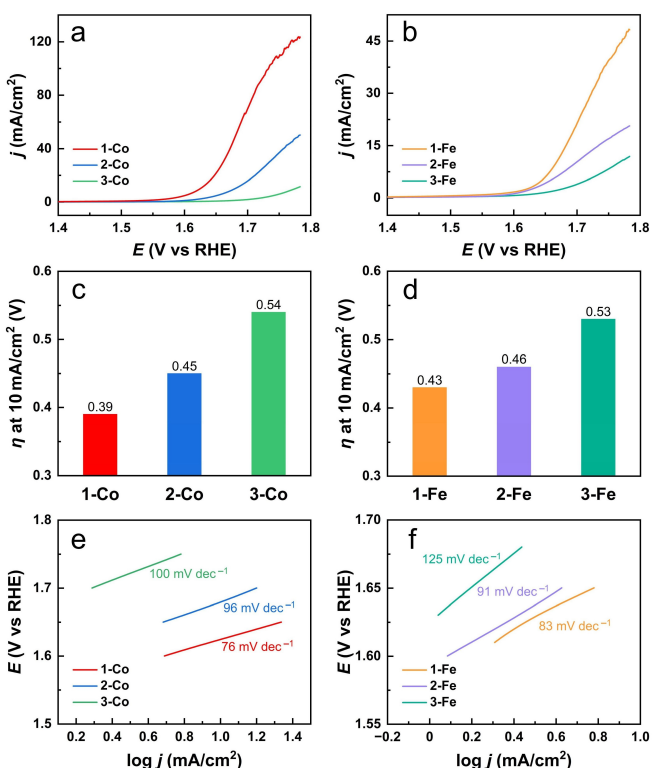


Figure 4. OER LSVs (a, b), η_{10} values (c, d), and Tafel slopes (e, f) of Co and Fe porphyrins. Conditions: 10 mV/s scan rate for LSV measurements; 2 mV/s scan rate for Tafel slope measurements.

their analogues (Figure 4e, 4f). Stability tests showed that **1-Co** (Figure S35) and **1-Fe** (Figure S36) were stable during OER electrolysis. The LSVs of **1-Co** (Figure S37) and **1-Fe** (Figure S38) before and after 1000 CV cycles showed negligible changes. The produced O₂ during the electrolysis was analyzed, giving Faraday efficiency of 96 % for OER (Figure S39, S40).

In heterogeneous electrocatalysis, catalytic performance may be affected by many factors. To address the difference of the OER activity of these metal porphyrins, we first determined that their catalyst loadings on CNTs are almost identical (Table S3). We then measured the electrochemical active surface area (ECSA). As shown in Figure S41–S44, the ECSA of catalyst-loaded CNTs is very similar to each other (Table S4). Moreover, for either Co- or Fe-loaded CNTs, the hybrids showed very similar electroactive molecules using the methods established in literature (Figure S45 and S46, Table S5).^[59] In addition, for either Co- or Fe-loaded CNTs, they have very similar electrical resistance and hydrophilic properties (Figure S47–S49). Therefore, these metal porphyrins have similar loading features on CNTs, which indicated that their different OER activities are due to their different structures. In addition, we synthesized **4-Co** and **4-Fe** (Scheme S2), in which the four *meso*-phenyl substituents each has an *ortho*-amido group. As we expected, **1-Co** and **4-Co** have similar redox properties (Table S1). However, **1-Co** is much more efficient than **4-Co** to electrocatalyze OER (Figure S50). Similar result

was observed for **1-Fe** and **4-Fe** (Figure S51). These results suggested that the tethered cyclen is essential to significantly improve the OER activity of Co and Fe porphyrins.

We hypothesized that the axial coordination of metal ions play a crucial role in O–O bond formation. To study this effect, we used density functional theory (DFT) calculations. In alkaline solutions, hydroxide nucleophilic attack on formal $M^{IV}=O$ and $M^V=O$ was considered to form an O–O bond. As shown in Figure 5, the O–O bond formation barriers for **1-M** are smaller than those for **2-M**. In addition, Co-mediated O–O bond formation barriers are smaller than Fe-mediated ones. These results are consistent with experimental results. Compared to $M^{IV}=O$, hydroxide nucleophilic attack on formal $M^V=O$ occurs with substantially decreased energy barriers. Therefore, we will focus subsequent discussions on formal $M^V=O$ species. With an unoccupied *trans* axial site, the positive charge of $M^V=O$ moiety (labeled as C_{M-O}) in **1-M**, as determined by natural population analysis (NPA), is larger than that in **2-M**. More positively charged $M^V=O$ units of **1-M** is more favoured for the subsequent hydroxide nucleophilic attack.

Importantly, spin density distribution analysis of formal $M^V=O$ species showed that for **1-M**, few spin densities were distributed on the porphyrin plane, indicating a tetravalent metal ion with an oxyl ligand. On the contrary, for **2-M**, substantial spin densities on the porphyrin ligand were identified, suggesting a trivalent metal ion combined with a porphyrin cation radical and an oxyl ligand. Compared to **2-M**, the metal ion of formal $M^V=O$ in **1-M** has a higher valence state, leading to more positively charged metal-oxo units. Structural analysis of $M^V=O$ showed that the N–N–N–M dihedral angle in **1-M** is larger than that in **2-M**.

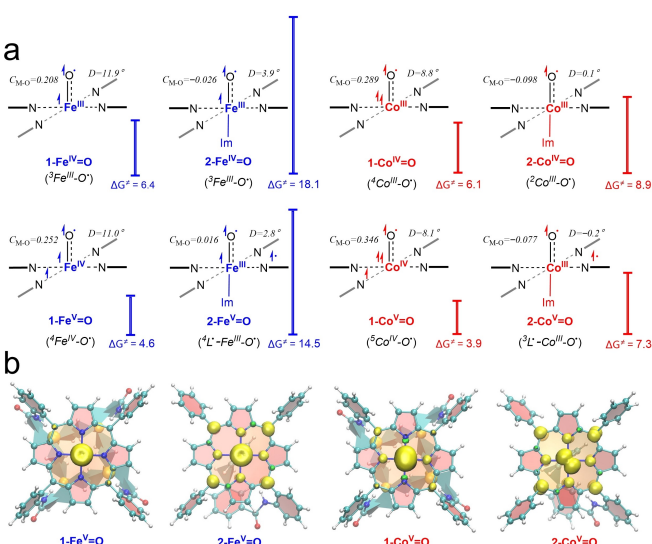


Figure 5. (a) Schematic demonstration of metal-oxo species and corresponding O–O bond formation barriers (in kcal/mol) through hydroxide nucleophilic attack. (b) The spin density distributions of formal $M^V=O$ species (isovalue is 0.005). The unpaired electrons are depicted as half arrows. The N–N–N–M dihedral angle (labeled as D) and the atomic NPA charge of the M–O moiety (labeled as C_{M-O}) are also provided.

This result suggests that the metal ion of $M^V=O$ in **1-M** has a larger doming effect as compared to **2-M**. Because of the larger doming effect, the orbital overlap between the metal center and the porphyrin ligand in **1-M** is relatively smaller. However, the more planar $M-N_4$ structure of the formal $M^V=O$ unit in **2-M** causes better orbital overlaps between the metal ion and the porphyrin ligand, making its porphyrin ligand more redox non-innocent and thus decrease the positive charge of the metal ion. Therefore, in addition to the electronic “push effect” of *trans* axial ligand, the doming effect enables more positive charge locating at the metal ion for formal $M^V=O$ in **1-M**. These effects together cause more positively charged metal-oxo for nucleophilic attack. This ligand field effect on the O–O bond formation has been rarely studied and is of fundamental significance.

In conclusion, we report on the design and synthesis of **1-M** with a coordinatively unsaturated metal center for improved OER. With a tethered cyclen, this protected metal axial site will maintain unoccupied during OER as suggested from crystallographic and spectrographic studies. We show that **1-Co** and **1-Fe** are more active for OER than analogues lacking such an axial protection. In addition to the electronic “push effect” of *trans* axial ligand, we further demonstrated that the doming effect of metal-oxo plays a critical role in regulating the charge distribution between the metal ion and porphyrin. This work is therefore significant to show axial coordination tuning effects on O–O bond formation and to present an unparalleled strategy to synthesize coordinatively unsaturated metal porphyrins for improved OER.

Acknowledgements

We are grateful for the support from the National Natural Science Foundation of China (21773146, 22003036 and 22171176), the Fok Ying-Tong Education Foundation for Outstanding Young Teachers in University, Fundamental Research Funds for the Central Universities (GK202103033), and the Research Funds of Shaanxi Normal University (2021TS027). U.-P. A. is grateful for the Fraunhofer Internal Programs under Grant No. Attract 097-602175 and the DFG under Germany’s Excellence Strategy-EXC-2033-Projektnummer 390677874 “RESOLV”.

Conflict of Interest

The authors declare no conflict of interest.

Data Availability Statement

The data that support the findings of this study are available in the supplementary material of this article.

Keywords: Axial Ligand Effect · Coordination Tuning · Molecular Electrocatalysis · O–O Bond Formation · Oxygen Evolution

- [1] R. D. Britt, D. A. Marchiori, *Science* **2019**, *366*, 305–306.
- [2] M. Kondo, H. Tatewaki, S. Masaoka, *Chem. Soc. Rev.* **2021**, *50*, 6790–6831.
- [3] W. Zhang, W. Lai, R. Cao, *Chem. Rev.* **2017**, *117*, 3717–3797.
- [4] D. K. Dogutan, D. G. Nocera, *Acc. Chem. Res.* **2019**, *52*, 3143–3148.
- [5] B. Zhang, L. Sun, *Chem. Soc. Rev.* **2019**, *48*, 2216–2264.
- [6] R. Matheu, P. Garrido-Barros, M. Gil-Sepulcre, M. Z. Ertem, X. Sala, C. Gimbert-Suriñach, A. Llobet, *Nat. Chem. Rev.* **2019**, *3*, 331–341.
- [7] H. Yang, F. Li, S. Zhan, Y. Liu, W. Li, Q. Meng, A. Kravchenko, T. Liu, Y. Yang, Y. Fang, L. Wang, J. Guan, I. Furó, M. S. G. Ahlquist, L. Sun, *Nat. Catal.* **2022**, *5*, 414–429.
- [8] J. Li, C. A. Triana, W. Wan, D. P. Adiyeri Saseendran, Y. Zhao, S. E. Balaghi, S. Heidari, G. R. Patzke, *Chem. Soc. Rev.* **2021**, *50*, 2444–2485.
- [9] W.-C. Hsu, Y.-H. Wang, *ChemSusChem* **2022**, *15*, e202102378.
- [10] L. Gao, X. Cui, C. D. Sewell, J. Li, Z. Lin, *Chem. Soc. Rev.* **2021**, *50*, 8428–8469.
- [11] V. Artero, *Nat. Energy* **2017**, *2*, 17131.
- [12] N. Wang, P. Ou, S.-F. Hung, J. E. Huang, A. Ozden, J. Abed, I. Grigioni, C. Chen, R. K. Miao, Y. Yan, J. Zhang, Z. Wang, R. Dorakhan, A. Badreldin, A. Abdel-Wahab, D. Sinton, Y. Liu, H. Liang, E. H. Sargent, *Adv. Mater.* **2023**, *35*, 2210057.
- [13] G. Righi, J. Plescher, F.-P. Schmidt, R. K. Campen, S. Fabris, A. Knop-Gericke, R. Schlögl, T. E. Jones, D. Teschner, S. Piccinin, *Nat. Catal.* **2022**, *5*, 888–899.
- [14] Z.-Y. Wu, F.-Y. Chen, B. Li, S.-W. Yu, Y. Z. Finfrock, D. M. Meira, Q.-Q. Yan, P. Zhu, M.-X. Chen, T.-W. Song, Z. Yin, H.-W. Liang, S. Zhang, G. Wang, H. Wang, *Nat. Mater.* **2023**, *22*, 100–108.
- [15] Y. Zhao, X. F. Lu, Z.-P. Wu, Z. Pei, D. Luan, X. W. Lou, *Adv. Mater.* **2023**, *35*, 2207888.
- [16] V. Artero, M. Fontecave, *Chem. Soc. Rev.* **2013**, *42*, 2338–2356.
- [17] L. Chen, G. Chen, C.-F. Leung, C. Cometto, M. Robert, T.-C. Lau, *Chem. Soc. Rev.* **2020**, *49*, 7271–7283.
- [18] X.-P. Zhang, A. Chandra, Y.-M. Lee, R. Cao, K. Ray, W. Nam, *Chem. Soc. Rev.* **2021**, *50*, 4804–4811.
- [19] Y. Liu, T.-C. Lau, *J. Am. Chem. Soc.* **2019**, *141*, 3755–3766.
- [20] B. Battistella, K. Ray, *Coord. Chem. Rev.* **2020**, *408*, 213176.
- [21] N. Noll, A.-M. Krause, F. Beuerle, F. Würthner, *Nat. Catal.* **2022**, *5*, 867–877.
- [22] M. Suga, F. Akita, K. Yamashita, Y. Nakajima, G. Ueno, H. Li, T. Yamane, K. Hirata, Y. Umena, S. Yonekura, L.-J. Yu, H. Murakami, T. Nomura, T. Kimura, M. Kubo, S. Baba, T. Kumasaka, K. Tono, M. Yabashi, H. Isobe, K. Yamaguchi, M. Yamamoto, H. Ago, J.-R. Shen, *Science* **2019**, *366*, 334–338.
- [23] C. Casadevall, V. Martin-Diaconescu, W. R. Browne, S. Fernández, F. Franco, N. Cabello, J. Benet-Buchholz, B. Lassalle-Kaiser, J. Lloret-Fillol, *Nat. Chem.* **2021**, *13*, 800–804.
- [24] Y. Guo, J. Messinger, L. Kloof, L. Sun, *J. Am. Chem. Soc.* **2022**, *144*, 11736–11747.
- [25] X.-P. Zhang, H.-Y. Wang, H. Zheng, W. Zhang, R. Cao, *Chin. J. Catal.* **2021**, *42*, 1253–1268.
- [26] X. Li, X.-P. Zhang, M. Guo, B. Lv, K. Guo, X. Jin, W. Zhang, Y.-M. Lee, S. Fukuzumi, W. Nam, R. Cao, *J. Am. Chem. Soc.* **2021**, *143*, 14613–14621.
- [27] L. Xie, X.-P. Zhang, B. Zhao, P. Li, J. Qi, X. Guo, B. Wang, H. Lei, W. Zhang, U.-P. Apfel, R. Cao, *Angew. Chem. Int. Ed.* **2021**, *60*, 7576–7581.
- [28] T. Ghosh, G. Maayan, *Angew. Chem. Int. Ed.* **2019**, *58*, 2785–2790.
- [29] G. Maayan, N. Gluz, G. Christou, *Nat. Catal.* **2018**, *1*, 48–54.
- [30] L. Schwiedrzik, T. Rajkovic, L. González, *ACS Catal.* **2023**, *13*, 3007–3019.
- [31] M. Okamura, M. Kondo, R. Kuga, Y. Kurashige, T. Yanai, S. Hayami, V. K. K. Praneeth, M. Yoshida, K. Yoneda, S. Kawata, S. Masaoka, *Nature* **2016**, *530*, 465–468.
- [32] Z. Codolà, I. Gamba, F. Acuña-Parés, C. Casadevall, M. Clémancey, J.-M. Latour, J. M. Luis, J. Lloret-Fillol, M. Costas, *J. Am. Chem. Soc.* **2019**, *141*, 323–333.
- [33] H.-T. Zhang, X.-J. Su, F. Xie, R.-Z. Liao, M.-T. Zhang, *Angew. Chem. Int. Ed.* **2021**, *60*, 12467–12474.
- [34] W. Sinha, A. Mahammed, N. Fridman, Z. Gross, *ACS Catal.* **2020**, *10*, 3764–3772.
- [35] B. Mondal, S. Chattopadhyay, S. Dey, A. Mahammed, K. Mittra, A. Rana, Z. Gross, A. Dey, *J. Am. Chem. Soc.* **2020**, *142*, 21040–21049.
- [36] L. Xie, X. Li, B. Wang, J. Meng, H. Lei, W. Zhang, R. Cao, *Angew. Chem. Int. Ed.* **2019**, *58*, 18883–18887.
- [37] A. I. Nguyen, K. M. Van Allsburg, M. W. Terban, M. Bajdich, J. Oktawiec, J. Amtawong, M. S. Ziegler, J. P. Dombrowski, K. V. Lakshmi, W. S. Drisdell, J. Yano, S. J. L. Billinge, T. D. Tilley, *Proc. Natl. Acad. Sci. USA* **2019**, *116*, 11630–11639.
- [38] H. Liu, H. Frei, *ACS Catal.* **2020**, *10*, 2138–2147.
- [39] A. Aljabour, H. Awada, L. Song, H. Sun, S. Offenthaler, F. Yari, M. Bechmann, M. C. Scharber, W. Schöfberger, *Angew. Chem. Int. Ed.* **2023**, *62*, e202302208.
- [40] H. Lei, Q. Zhang, Z. Liang, H. Guo, Y. Wang, H. Lv, X. Li, W. Zhang, U.-P. Apfel, R. Cao, *Angew. Chem. Int. Ed.* **2022**, *61*, e202201104.
- [41] J. Hessels, E. Masferrer-Rius, F. Yu, R. J. Detz, R. J. M. Klein Gebbink, J. N. H. Reek, *ChemSusChem* **2020**, *13*, 6629–6634.
- [42] H.-T. Zhang, Y.-H. Guo, Y. Xiao, H.-Y. Du, M.-T. Zhang, *Angew. Chem. Int. Ed.* **2023**, *62*, e202218859.
- [43] P. Garrido-Barros, S. Grau, S. Drouet, J. Benet-Buchholz, C. Gimbert-Suriñach, A. Llobet, *ACS Catal.* **2019**, *9*, 3936–3945.
- [44] Q.-F. Chen, Z.-Y. Cheng, R.-Z. Liao, M.-T. Zhang, *J. Am. Chem. Soc.* **2021**, *143*, 19761–19768.
- [45] P. Garrido-Barros, D. Moonshiram, M. Gil-Sepulcre, P. Pelosin, C. Gimbert-Suriñach, J. Benet-Buchholz, A. Llobet, *J. Am. Chem. Soc.* **2020**, *142*, 17434–17446.
- [46] Y. Liu, Y. Han, Z. Zhang, W. Zhang, W. Lai, Y. Wang, R. Cao, *Chem. Sci.* **2019**, *10*, 2613–2622.
- [47] M. Gil-Sepulcre, P. Garrido-Barros, J. Oldengott, I. Funes-Ardoiz, R. Bofill, X. Sala, J. Benet-Buchholz, A. Llobet, *Angew. Chem. Int. Ed.* **2021**, *60*, 18639–18644.
- [48] G. Mukherjee, J. K. Satpathy, U. K. Bagha, M. Q. E. Mubarak, C. V. Sastri, S. P. de Visser, *ACS Catal.* **2021**, *11*, 9761–9797.
- [49] S. Yokota, Y. Suzuki, S. Yanagisawa, T. Ogura, S. Nozawa, M. Hada, H. Fujii, *ACS Catal.* **2022**, *12*, 10857–10871.
- [50] M. Guo, Y.-M. Lee, S. Fukuzumi, W. Nam, *Coord. Chem. Rev.* **2021**, *435*, 213807.
- [51] M. Guo, T. Corona, K. Ray, W. Nam, *ACS Cent. Sci.* **2019**, *5*, 13–28.
- [52] Crystal data for **d**: [C₆₆H₆₄Cl₆N₁₂O₇], Tetragonal, *I*̄₄, *a* = 27.7541 (18) Å, *c* = 16.8033(15) Å, *V* = 12943(2) Å³, *Z* = 8, *T* = 153(2) K, 74904 reflections collected, 11809 unique (*R*_{int}) = 0.0375, final *R*1 = 0.0879, *wR*2 = 0.2563 for 11365 observed reflections [*I* > 2σ(*I*)]. Deposition number 2212700 contains the supplementary crystallographic data for this paper. These data are provided free of charge by the joint Cambridge Crystallographic Data Centre and Fachinformationszentrum Karlsruhe Access Structures service.
- [53] Crystal data for **1-Co**: [C₆₆H₆₅Cl₆CoN₁₂O₅], Monoclinic, *P*2₁/c, *a* = 16.7878(12) Å, *b* = 17.0940(16) Å, *c* = 25.721(2) Å, *β* = 107.864(3)°, *V* = 7025.3(10) Å³, *Z* = 4, *T* = 153(2) K, 63835 reflections collected, 12359 unique (*R*_{int}) = 0.0527, final *R*1 = 0.0793, *wR*2 = 0.2799 for 10384 observed reflections [*I* > 2σ(*I*)]. Deposition number 2212629 contains the supplementary crystallographic data for this paper. These data are provided free of charge by the joint Cambridge Crystallographic Data Centre and Fachinformationszentrum Karlsruhe Access Structures service.

- free of charge by the joint Cambridge Crystallographic Data Centre and Fachinformationszentrum Karlsruhe Access Structures service.
- [54] Crystal data for **1-Fe** dimer: [C₁₃₀H₁₂₄Cl₄Fe₂N₂₄O₁₉], Tetragonal, P4nc, $a=16.670(2)$ Å, $c=23.229(4)$ Å, $V=6455.1(19)$ Å³, Z=2, $T=153(2)$ K, 80023 reflections collected, 5924 unique ($R_{\text{int}}=0.1002$, final $R1=0.0961$, wR2=0.2443 for 5522 observed reflections [$I>2\sigma(I)$]). Deposition number 2212627 contains the supplementary crystallographic data for this paper. These data are provided free of charge by the joint Cambridge Crystallographic Data Centre and Fachinformationszentrum Karlsruhe Access Structures service.
- [55] C. Zhang, P. Gotico, R. Guillot, D. Dragoe, W. Leibl, Z. Halime, A. Aukauloo, *Angew. Chem. Int. Ed.* **2023**, *62*, e202214665.
- [56] J. Yang, P. Li, X. Li, L. Xie, N. Wang, H. Lei, C. Zhang, W. Zhang, Y.-M. Lee, W. Zhang, R. Cao, S. Fukuzumi, W. Nam, *Angew. Chem. Int. Ed.* **2022**, *61*, e202208143.
- [57] H. Kim, P. J. Rogler, S. K. Sharma, A. W. Schaefer, E. I. Solomon, K. D. Karlin, *J. Am. Chem. Soc.* **2020**, *142*, 3104–3116.
- [58] S. Yokota, H. Fujii, *J. Am. Chem. Soc.* **2018**, *140*, 5127–5137.
- [59] R. Matheu, E. Gutierrez-Puebla, M. Á. Monge, C. S. Diercks, J. Kang, M. S. Prévot, X. Pei, N. Hanikel, B. Zhang, P. Yang, O. M. Yaghi, *J. Am. Chem. Soc.* **2019**, *141*, 17081–17085.

Manuscript received: April 27, 2023

Accepted manuscript online: August 7, 2023

Version of record online: August 16, 2023